

LayoutDETR: Detection Transformer Is a Good Multimodal Layout Designer

Ning Yu Chia-Chih Chen Zeyuan Chen Rui Meng Gang Wu Paul Josel
 Juan Carlos Niebles Caiming Xiong Ran Xu
 Salesforce Research

{ning.yu, chiachih.chen, zeyuan.chen, ruimeng, gang.wu
 pjosel, jniebles, cxiong, ran.xu}@salesforce.com

Abstract

Graphic layout designs play an essential role in visual communication. Yet handcrafting layout designs are skill-demanding, time-consuming, and non-scalable to batch production. Although generative models emerge to make design automation no longer utopian, it remains non-trivial to customize designs that comply with designers’ multimodal desires, i.e., constrained by background images and driven by foreground contents. In this study, we propose *LayoutDETR* that inherits the high quality and realism from generative modeling, in the meanwhile reformulating content-aware requirements as a detection problem: we learn to detect in a background image the reasonable locations, scales, and spatial relations for multimodal elements in a layout. Experiments validate that our solution yields new state-of-the-art performance for layout generation on public benchmarks and on our newly-curated ads banner dataset. For practical usage, we build our solution into a graphical system that facilitates user studies. We demonstrate that our designs attract more subjective preferences than baselines by significant margins. Our code, models, dataset, graphical system, and demos are available at [GitHub](#).

1. Introduction

Graphic layout designs are at the foundation of communication between media designers and their target audience (Lok & Feiner, 2001; Landa, 2010; Stribley, 2016). Multimodal elements, i.e., foreground images/texts, are framed by layout bounding boxes and reasonably arranged on a background image. This relies on thoughtful understanding of the semantics of each element and their harmony as a whole. As a result, handcrafting such layout designs is skill-demanding, time-consuming, and requires hiring experienced professionals. It is even impossible to handle batch production in a massive quantity (Chen et al., 2019).

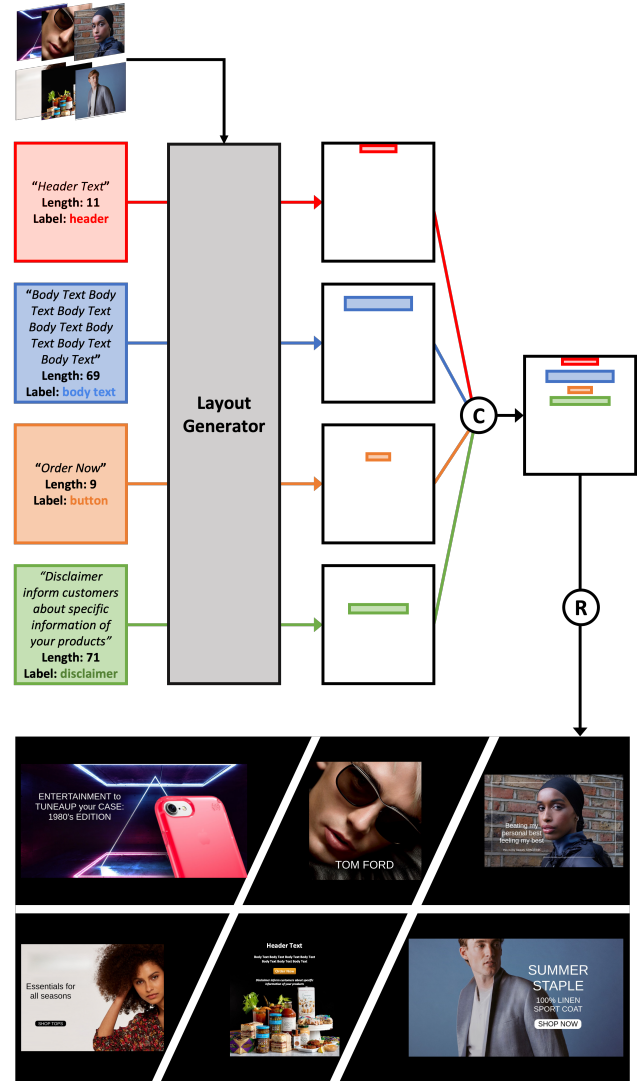


Figure 1. **Top:** LayoutDETR takes a background image and a set of multimodal foreground elements (images/texts) as inputs, and outputs an aesthetically appealing layout. **Bottom:** we showcase a few ads banner samples with rendered texts following our auto-designed layouts. “C” indicates the composition process. “R” indicates the rendering process.

Motivated by the growing demands of automating graphic layout designs, researchers adapt the emerging advances of deep generative models (Goodfellow et al., 2014; Kingma & Welling, 2013; Larsen et al., 2016; Chen et al., 2018) to this task (Li et al., 2019; Kikuchi et al., 2021; Zheng et al., 2019; Patil et al., 2020; Guo et al., 2021; Gupta et al., 2021; Kong et al., 2022; Zhou et al., 2022; Cao et al., 2022). Unfortunately, few of them investigate the multimodal nature of input conditions and how to fuse them for layout designs.

Multimodal conditions are critical to enrich designers’ control and command the aesthetics of layout designs. In this paper, we put a focused lens on them. We propose to equip designers with an AI-empowered system that allows multimodal input: arbitrary background images, foreground images, and foreground copywriting texts from varying categories. Figure 1 depicts the functionality and resulting design samples of our solution. We learn a generative model of conditional layout distribution that is constrained by background images and driven by foreground elements. Technically, it requires our model to (1) learn the prior distribution from large-scale realistic layout samples, (2) understand the appearances and semantics of background images, (3) understand the appearances and semantics of foreground elements, and (4) interact across the background and multiple foreground elements to generate the layout bounding box parameters of each foreground element.

To handle (1), we inherit and explore the high-realism success from three types of generative learning paradigms as aforementioned: generative adversarial networks (GANs) (Goodfellow et al., 2014; Karras et al., 2020), variational autoencoders (VAEs) (Kingma & Welling, 2013), and VAE-GAN (Larsen et al., 2016). To handle (2), we reformulate the background conditioned layout generation as a detection problem, considering both problems require visual understanding of an image and optimize for bounding box parameters. We integrate these two seemingly irrelevant techniques and train a DETR-flavored detector (Carion et al., 2020) as a layout generator. Specifically, we employ the visual transformer encoder and bounding box transformer decoder architectures of DETR. We jointly optimize its supervision loss with generative adversarial loss. We hence name our solution *LayoutDETR*. To handle (3), we incorporate a CNN-based image encoder (Caron et al., 2020) and a BERT-based text encoder (Devlin et al., 2019) for the multimodal foreground inputs, and feed the features as input tokens to DETR transformer decoder. (4) is naturally handled by DETR thanks to its transformer nature: Foreground elements interact with each other through the self-attention layers in the decoder, while background features interact through the cross-attention layers between the image encoder and layout decoder.

We summarize our **contributions** in four thrusts:

(1) **Method.** We bridge two seemingly irrelevant research domains, layout generation and visual detection, into one framework that solves multimodal graphic layout design constrained by background images and driven by foreground images/texts. No existing methods are able to handle all these modalities at once.

(2) **Dataset.** We establish a large-scale ads banner dataset with rich semantic annotations including text bounding boxes, text categories, and text contents. We then benchmark this dataset for graphic layout generation over four baseline methods, three of our solution variants, and conduct ablation study.

(3) **State-of-the-art performance.** Our solution sets up new state-of-the-art performance for graphic layout generation by a comprehensive set of six evaluation metrics, which measure the realism, accuracy, and regularity of generated layouts.

(4) **Graphical system and user study.** For practical usage, we further build our solution into a graphical system that scales up layout generation and facilitates user study. We showcase to users generated layout samples like in Figure 1 bottom. Users’ feedback reflects that our designs attract more subjective preferences than all baselines by significant margins.

2. Related Work

2.1. Deep Generative Models for Layout Design

Automating the design of layouts with high quality and realism gains increasing attention and achieves substantial progress, thanks to the revolutionary advancements of deep generative models, especially generative adversarial networks (GANs) (Goodfellow et al., 2014; Brock et al., 2019; Karras et al., 2018; 2019; 2020; Yu et al., 2020; 2021; Sauer et al., 2022; Lee et al., 2022; Yu et al., 2022), variational autoencoders (VAEs) (Kingma & Welling, 2013; Rezende et al., 2014; Larsen et al., 2016), and autoregressive models (ARMs) (Van den Oord et al., 2016; Salimans et al., 2017; Chen et al., 2018). Researchers adopt generative models to learn to generate bounding box parameters, in the form of center location, height, width, and optionally depth, for each foreground element in a layout in either graphics or natural scene domains. Orthogonal to learning paradigms, existing methods also investigate a variety of generator architectures including multi-layer perceptron (MLP) (Krizhevsky et al., 2012), convolutional neural networks (CNN) (Simonyan & Zisserman, 2015), recursive neural networks (RvNN) (Socher et al., 2011; 2013), long short-term memory (LSTM) (Hochreiter & Schmidhuber, 1997; Haykin & Network, 2004), graph convolutional networks (GCN) (Kipf & Welling, 2017), and transformer (Vaswani et al., 2017; Devlin et al., 2019). Some layout design methods (Li et al., 2019; 2020; Kikuchi et al., 2021; Jyothi et al., 2019; Zheng

et al., 2019; Patil et al., 2020; Lee et al., 2020; Guo et al., 2021; Nguyen et al., 2021; Xie et al., 2021; Gupta et al., 2021; Arroyo et al., 2021; Kong et al., 2022; Yamaguchi, 2021; Jiang et al., 2022b; Wang et al., 2022; Zhou et al., 2022; Cao et al., 2022; Jiang et al., 2022a) focus on graphics domain only, while others (Jyothi et al., 2019; Arroyo et al., 2021; Gupta et al., 2021; Kong et al., 2022; Tan et al., 2018; Zhao et al., 2018; Lee et al., 2018) generalize to natural scenes or even 3D data. Some methods (Li et al., 2019; Kikuchi et al., 2021; Patil et al., 2020; Gupta et al., 2021; Kong et al., 2022) allow only bounding box category condition, while others (Li et al., 2020; Lee et al., 2020; Zheng et al., 2019; Guo et al., 2021; Zhou et al., 2022; Cao et al., 2022) allow richer conditions in multi-modalities, typically in the forms of background images, foreground images, or copywriting texts, but not all. See a comprehensive taxonomy of layout generation methods in Table 4 in the supplementary material.

None of the existing multimodal layout generation methods (Li et al., 2020; Lee et al., 2020; Zheng et al., 2019; Guo et al., 2021; Zhou et al., 2022; Cao et al., 2022) is designed to handle all the background and foreground modalities at once. LayoutGAN+ (Li et al., 2020) and NDN (Lee et al., 2020) do not involve image elements in their formulation. CGL-GAN (Zhou et al., 2022) and ICVT (Cao et al., 2022) do not involve text elements in their formulation. ContentGAN (Zheng et al., 2019) does not take layout information for training and does not even use complete background images as input during training. This does not benefit the layout representation, layout regularity, or final quality (e.g., text readability) after rendering foreground elements onto the background. Vinci (Guo et al., 2021) largely relies on a finite set of predefined layout candidates to choose background images from a pool of food and beverage domains. Their method is unable to design layouts conditioned on arbitrary backgrounds in open domains, natural or handcrafted, plain or cluttered, like ours. Considering multimodal layout design persists as a challenging problem, we focus our exclusive scope on graphic layouts, e.g., mobile application UIs and our newly-organized large-scale ads banners.

2.2. Object Detection

The goal of object detection is to predict a set of bounding boxes and their categories for each object of interest in a query image. Modern detectors address this in one of three ways: Two-stage detectors (Girshick, 2015; Ren et al., 2015; He et al., 2017) predict boxes based on proposals; single-stage detectors predict boxes based on anchors (Lin et al., 2017) or a grid of possible object centers (Redmon et al., 2016; Redmon & Farhadi, 2017); direct detectors (Carion et al., 2020; Dai et al., 2021; Meng et al., 2021; Liu et al., 2022) get rid of those hand-crafted initial guesses and directly predict absolute parameters of boxes w.r.t. query

images.

The direct detectors (Carion et al., 2020; Dai et al., 2021) inspire us to leverage their powerful image understanding capability, and combine it with modern layout generators, in order to address the problem of multimodal layout generation. Similar in the spirit of CGL-GAN (Zhou et al., 2022) or ICVT (Cao et al., 2022), we take full advantage of the transformer encoder-decoder architecture and generalized intersection over union (gIoU) loss (Rezatofighi et al., 2019) in DETR (Carion et al., 2020) to learn from background image context. Beyond CGL-GAN and ICVT, our layout outputs are altogether driven by foreground image/text conditions.

3. LayoutDETR for Multimodal Layout Design

3.1. Problem Statement

A graphic layout sample \mathcal{L} is represented by a set of N 2D bounding boxes $\{\mathbf{b}^i\}_{i=1}^N$. Each \mathbf{b}^i is parameterized by a vector with four elements: its center location in a background image (y^i, x^i) , height h^i , and width w^i . In order to handle background images \mathbf{B} with arbitrary sizes (H, W) , we normalize box parameters by their image size correspondingly, i.e., $\mathcal{L} = \{(y^i/H, x^i/W, h^i/Y, w^i/W)\}_{i=1}^N \doteq \{\hat{\mathbf{b}}^i\}_{i=1}^N$. Multimodal input conditions consist of the background image \mathbf{B} and a set of N foreground elements, in the form of either texts $\mathcal{T} = \{\mathbf{t}^i\}_{i=1}^M = \{(s^i, c^i, l^i)\}_{i=1}^M$ or image patches $\mathcal{P} = \{\mathbf{p}^i\}_{i=1}^K$, where $M \geq 0, K \geq 0, M+K = N$. s^i stands for the text string, c^i stands for the text class belonging to $\{\text{header text}, \text{body text}, \text{disclaimer text}, \text{button text}\}$, and l^i stands for the length of the text string. Each foreground element corresponds to a bounding box in the layout, indicating its location and size. Our goal is to learn a layout generator G that takes a latent noise vector \mathbf{z} and the multimodal conditions as input, and outputs a realistic and reasonable layout complying with the multimodal control: $G(\mathbf{z}, \mathbf{B}, \mathcal{T} \cup \mathcal{P}) \mapsto \mathcal{L}_{\text{fake}}$.

3.2. Generative Learning Frameworks

GAN variant. Following the GAN paradigm (Goodfellow et al., 2014; Brock et al., 2019; Karras et al., 2018; 2019; 2020; Yu et al., 2020; 2021; Sauer et al., 2022; Lee et al., 2022; Yu et al., 2022), the generator G is simultaneously and adversarially trained against discriminator D training. We formulate a multimodal-conditional discriminator $D^c(\mathcal{L}, \mathbf{B}, \mathcal{T} \cup \mathcal{P}) \mapsto \{0, 1\}$, as well as an unconditional discriminator $D^u(\mathcal{L}) \mapsto \{0, 1\}$.

In addition, it is observed that the discriminators are insensitive to irregular bounding box positions (Kikuchi et al., 2021). For example, the discriminators tend to overlook the unusual layout where a *header texts* is placed at the bottom. As a result, we follow the self-learning technique in (Liu

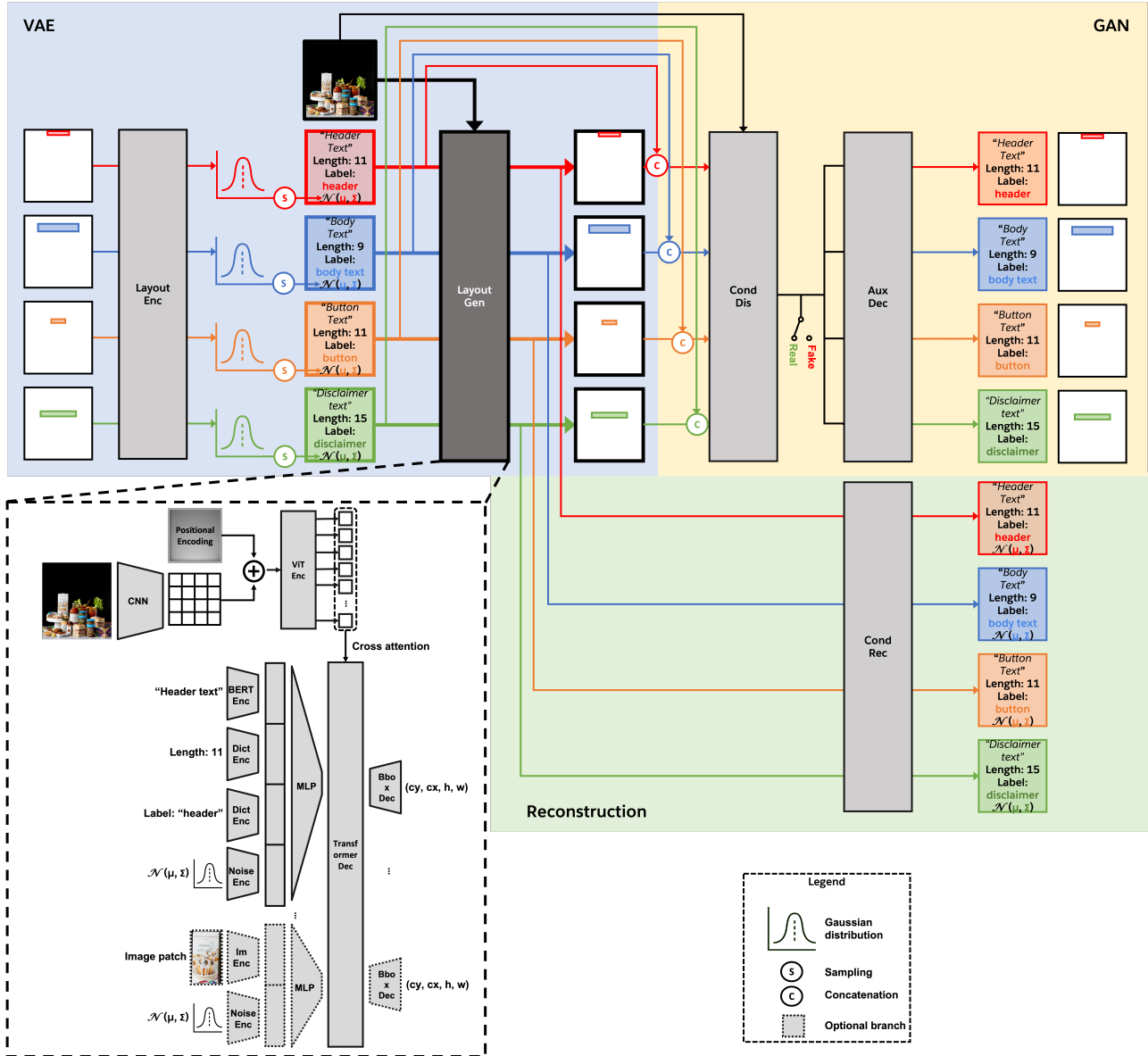


Figure 2. Our unified training framework covers three generator variants: GAN-, VAE-, and VAE-GAN-based. The layout generator network in a darker color and in bold appears in all the variants. Its DETR-based multimodal architecture is detailed at the bottom left. During inference, only the generator is needed.

et al., 2020) and add position-aware regularization to our discriminators. Specifically, similar in the spirit of (Kikuchi et al., 2021), we add an auxiliary decoder to each discriminator to reconstruct its input. The decoders F^c/F^u take the output features $\mathbf{f}^c/\mathbf{f}^u$ of their discriminators D^c/D^u , add them with learnable positional embeddings $\mathcal{E}^c = \{\mathbf{e}_i^c\}_{i=1}^N / \mathcal{E}^u = \{\mathbf{e}_i^u\}_{i=1}^N$, and reconstruct the bounding box parameters and multimodal conditions that are the input of the discriminators: $F^c(\mathbf{f}^c, \mathcal{E}^c) \mapsto \mathcal{L}_{\text{dec}}^c, \mathbf{B}_{\text{dec}}, \mathcal{T}_{\text{dec}} \cup \mathcal{P}_{\text{dec}}$; $F^u(\mathbf{f}^u, \mathcal{E}^u) \mapsto \mathcal{L}_{\text{dec}}^u$. The decoders are jointly trained with the discriminators to minimize the reconstruction loss. See Figure 2 Yellow for the diagram. To sum up, the adversarial learning objective is formulated as:

$$\begin{aligned} & \min_G \max_{D^c, F^c, \mathcal{E}^c, D^u, F^u, \mathcal{E}^u} L_{\text{GAN}} \\ & \doteq \mathbb{E}_{\mathbf{z} \sim \mathcal{N}(\mathbf{0}, \mathbf{I}), \{\mathbf{B}, \mathcal{T} \cup \mathcal{P}\} \sim P_{\text{data}}} \left[\log(1 - D^c(\mathcal{L}_{\text{fake}}, \mathbf{B}, \mathcal{T} \cup \mathcal{P})) \right. \\ & \left. + \log(1 - D^u(\mathcal{L}_{\text{fake}})) \right] \\ & + \mathbb{E}_{\{\mathcal{L}_{\text{real}}, \mathbf{B}, \mathcal{T} \cup \mathcal{P}\} \sim P_{\text{data}}} \left[\log(D^c(\mathcal{L}_{\text{real}}, \mathbf{B}, \mathcal{T} \cup \mathcal{P})) \right. \\ & \left. + \log(D^u(\mathcal{L}_{\text{real}})) \right] \\ & - L_{\text{dec}}(F^c(\mathbf{f}^c, \mathcal{E}^c), (\mathcal{L}_{\text{real}}, \mathbf{B}, \mathcal{T} \cup \mathcal{P})) \\ & - \lambda_{\text{layout}} L_{\text{layout}}(F^u(\mathbf{f}^u, \mathcal{E}^u, \mathcal{L}_{\text{real}})) \end{aligned} \quad (1)$$

$$\begin{aligned} & L_{\text{dec}}((\mathcal{L}_1, \mathbf{B}_1, \mathcal{T}_1 \cup \mathcal{P}_1), (\mathcal{L}_2, \mathbf{B}_2, \mathcal{T}_2 \cup \mathcal{P}_2)) \\ & = \lambda_{\text{layout}} L_{\text{layout}}(\mathcal{L}_1, \mathcal{L}_2) \\ & + \lambda_{\text{im}} (\|\mathbf{B}_1 - \mathbf{B}_2\|_2 + L_{\text{im}}(\mathcal{P}_1, \mathcal{P}_2)) + L_{\text{text}}(\mathcal{T}_1, \mathcal{T}_2) \end{aligned} \quad (2)$$

$$L_{\text{layout}}(\mathcal{L}_1, \mathcal{L}_2) = \frac{1}{N} \sum_{i=1}^N \|\hat{\mathbf{b}}_1^i - \hat{\mathbf{b}}_2^i\|_2 \quad (3)$$

$$L_{\text{im}}(\mathcal{P}_1, \mathcal{P}_2) = \frac{1}{N} \sum_{i=1}^N \|\mathbf{p}_1^i - \mathbf{p}_2^i\|_2 \quad (4)$$

$$\begin{aligned} & L_{\text{text}}(\mathcal{T}_1, \mathcal{T}_2) \\ & = \frac{1}{N} \sum_{i=1}^N (\lambda_{\text{str}} L_{\text{str}}(\mathbf{s}_1, \mathbf{s}_2) + \lambda_{\text{cls}} L_{\text{cls}}(c_1, c_2) + \lambda_{\text{len}} L_{\text{len}}(l_1, l_2)) \end{aligned} \quad (5)$$

$L_{\text{str}}, L_{\text{cls}}, L_{\text{len}}$ are the reconstruction losses for foreground text strings, text classes, and text lengths respectively. L_{str} is formulated as the auto-regressive loss according to BERT language modeling (Devlin et al., 2019; Li et al., 2022b). L_{cls} is the standard cross-entropy loss for classification. L_{len} is also the standard cross-entropy loss for classification, considering we quantize a string length integer scalar into 256 levels $[0, 255]$. $\lambda_{\text{layout}} = 500.0$, $\lambda_{\text{im}} = 0.5$, $\lambda_{\text{str}} = 0.1$,

$\lambda_{\text{cls}} = 50.0$, and $\lambda_{\text{len}} = 2.0$ are hyper-parameters used to balance each loss term in the same order of magnitude.

VAE variant. VAEs are an alternative paradigm to GANs for generative models. Following the VAE paradigm (Kingma & Welling, 2013; Rezende et al., 2014), the generator G is jointly trained with an encoder E that maps from the layout space to the latent noise distribution space. The output of E stands for the mean μ and covariance matrix Σ of a multivariate Gaussian distribution, $E(\mathcal{L}) \mapsto \mu, \Sigma$, the samples of which are input to G : $\text{sample}(\mu, \Sigma) = \mathbf{z}_0^T \Sigma^{\frac{1}{2}} \mathbf{z}_0 + \mu$, $\mathbf{z}_0 \sim \mathcal{N}(\mathbf{0}, \mathbf{I})$. It represents the differentiable reparameterization trick in the standard VAE pipeline (Kingma & Welling, 2013; Rezende et al., 2014). See Figure 2 Blue in the diagram.

The conditional VAE objective is to minimize the reconstruction loss:

$$\begin{aligned} \min_{E, G} L_{\text{VAE}} & \doteq \mathbb{E}_{\{\mathcal{L}_{\text{real}}, \mathbf{B}, \mathcal{T} \cup \mathcal{P}\} \sim P_{\text{data}}} \left[\lambda_{\text{layout}} L_{\text{layout}}(\mathcal{L}_{\text{fake}}, \mathcal{L}_{\text{real}}) \right. \\ & \left. + \lambda_{\text{KL}} \text{KL}(E(\mathcal{L}_{\text{real}}) \parallel \mathcal{N}(\mathbf{0}, \mathbf{I})) \right] \end{aligned} \quad (6)$$

$\text{KL}(\cdot \parallel \cdot)$ is the Kullback-Leibler (KL) Divergence used in standard VAE (Kingma & Welling, 2013; Rezende et al., 2014) to regularize the encoded latent noise distribution. The hyper-parameter $\lambda_{\text{KL}} = 1.0$.

VAE-GAN variant. VAEs and GANs are also compatible with each other. See Figure 2 Blue plus Yellow in the diagram. As suggested by (Larsen et al., 2016; Zheng et al., 2019), in this variant we jointly optimize Eq. 1 and Eq. 6:

$$\min_{E, G} \max_{D^c, F^c, \mathcal{E}^c, D^u, F^u, \mathcal{E}^u} L_{\text{GAN}} + L_{\text{VAE}} \quad (7)$$

3.3. Additional Objectives

Other losses and regularization terms also play important roles in the generated layout quality. First of all, we share the spirit with DETR (Carion et al., 2020) to add the bounding box supervision. We use the generalized intersection over union loss $\text{gIoU}(\cdot, \cdot)$ (Rezatofighi et al., 2019) between generated layout and its ground truth $L_{\text{gIoU}}(\mathcal{L}_{\text{fake}}, \mathcal{L}_{\text{real}})$, where:

$$L_{\text{gIoU}}(\mathcal{L}_1, \mathcal{L}_2) \doteq \lambda_{\text{gIoU}} \frac{1}{N} \sum_{i=1}^N \text{gIoU}(\hat{\mathbf{b}}_1^i, \hat{\mathbf{b}}_2^i) \quad (8)$$

where the hyper-parameter $\lambda_{\text{gIoU}} = 4.0$.

Second, we introduce an auxiliary reconstructor R for the generator to enhance the controllability of input conditions. R takes the last features of G , $\mathcal{F} = \{\mathbf{f}_i^g\}_{i=1}^N$, as input tokens before outputting box parameters, and learns to reconstruct \mathcal{P} and \mathcal{T} : $R(\mathcal{F}) \mapsto \mathcal{P}_{\text{rec}}, \mathcal{T}_{\text{rec}}$.

Jointly with G training, we learn to minimize:

$$L_{\text{rec}} \doteq \lambda_{\text{im}} L_{\text{im}}(\mathcal{P}_{\text{rec}}, \mathcal{P}_{\text{real}}) + L_{\text{text}}(\mathcal{T}_{\text{rec}}, \mathcal{T}_{\text{real}}) \quad (9)$$

where L_{im} refers to Eq. 4 and L_{text} refers to Eq. 5. See Figure 2 Green in the diagram.

Third, reasonable layout designs typically avoid overlapping between foreground elements. We follow (Li et al., 2020) to leverage their overlap loss (their Eq. 9) $L_{\text{overlap}} \doteq \lambda_{\text{overlap}} L_{\text{overlap}}(\mathcal{L}_{\text{fake}})$ that discourages overlapping between any pair of bounding boxes in a generated layout. The hyper-parameter $\lambda_{\text{overlap}} = 7.0$.

Fourth, aesthetically appealing layouts usually maintain one of the six alignments between a pair of adjacent bounding boxes: left, horizontal-center, right, top, vertical-center, and bottom aligned. We follow (Li et al., 2020) to leverage their misalignment loss (their Eq. 10) $L_{\text{misalign}} \doteq \lambda_{\text{misalign}} L_{\text{misalign}}(\mathcal{L}_{\text{fake}})$ that discourages misalignment. The hyper-parameter $\lambda_{\text{misalign}} = 17.0$.

Altogether our most complete combination of training objectives is formulated as follows:

$$\min_{E, G, R} \max_{D^c, F^c, \mathcal{E}^c, D^u, F^u, \mathcal{E}^u} L_{\text{GAN}} + L_{\text{VAE}} + L_{\text{gIoU}} + L_{\text{rec}} + L_{\text{overlap}} + L_{\text{misalign}} \quad (10)$$

3.4. DETR-based Multimodal Architectures

Architecture design is where we integrate object detection with layout generation. Detection transformer (DETR) (Carion et al., 2020) is employed and modified for LayoutDETR generator G and conditional discriminator D^c .

As depicted in Figure 2 bottom left, G and D^c contain a background encoder and a layout transformer decoder. The encoder is the same as in DETR (Carion et al., 2020). The decoder is inherited from the DETR decoder with self-attention and encoder-decoder-cross-attention mechanisms (Vaswani et al., 2017). Different from DETR, we replace their freely-learnable object queries with our foreground embeddings as the input tokens to the decoder. The decoder then transforms the embeddings to layout bounding box parameters. Foreground embedding is a concatenation of noise embedding and text/image embedding. Text embedding is a concatenation of text string embedding (BERT-pretrained and fixed), text class embedding (via learning dictionary), and text length embedding (via learning dictionary). See more details and implementations of the other networks in Section B in the supplementary material. In particular, other networks are transformer-based as well. Only the input and output formats differ depending on the network functionality. Note that we do not choose a wireframe discriminator considering its empirical performance is worse, the same observation as in (Kikuchi et al., 2021).

4. New Ads Banner Dataset

Not all existing datasets are suitable for multimodal layout design because they do not always provide multi-modality information, e.g. natural scene datasets. Other datasets, such as PubLayNet document dataset (Zhong et al., 2019) and PartNet 3D shape dataset (Yu et al., 2019) render layouts only on plain background. Magazine dataset (Zheng et al., 2019) does not provide complete background images since they have masked out foreground layouts from the background. On the other hand, ads banner datasets are composed of multimodal elements and lead to several previous layout design techniques (Guo et al., 2021; Lee et al., 2020; Kong et al., 2022; Zhou et al., 2022; Cao et al., 2022). Unfortunately, none of their datasets is publicly available, except for CGL dataset (Zhou et al., 2022) which yet does not contain English modality. We therefore collect a new large-scale ads banner dataset with 7,196 samples.

Each of our samples consists of a well-designed banner image, its layout ground truth, foreground text strings, text classes, and background image. The banner images are filtered from Pitt Image Ads Dataset (Hussain et al., 2017) and crawled from Google Image Search Engine. Their layouts and text classes are manually annotated by Amazon Mechanical Turk (AMT). The text classes span as $\{\text{header text}, \text{body text}, \text{disclaimer text}, \text{button text}\}$, and logos are categorized as *header text*. The text strings are extracted by a modern optical character recognition (OCR) technique¹, and erased by a modern image inpainting technique (Suvorov et al., 2022) to obtain the text-free background image. Examples and more details about data collection are in Section C, Figure 5 and 6 in the supplementary material.

5. Experiments

5.1. Setup

Datasets. Ablation study and user study are conducted on our newly-curated ads banner dataset with 7,196 samples. Comparisons to baselines are additionally performed on the recent CLAY dataset with 32,063 mobile application UI samples (Li et al., 2022a). It is a much cleaner version of the Rico dataset (Deka et al., 2017). Besides background image and foreground text conditions, it also involves foreground image conditions. We apply the same image inpainting process to separate CLAY foreground and background. 90% of the samples are used for training and 10% for testing.

Baselines. We select four recent state-of-the-art baseline methods covering a variety of generative paradigms and architectures according to the related work: LayoutGAN++ (Kikuchi et al., 2021) (GAN paradigm, transformer architecture), READ (Patil et al., 2020) (VAE paradigm, RvNN architecture), Vinci (Guo et al., 2021)

¹<https://github.com/PaddlePaddle/PaddleOCR>

(VAE paradigm, LSTM architecture), and LayoutTransformer (Gupta et al., 2021) (ARM paradigm, transformer architecture). We noted that LayoutTransformer (Gupta et al., 2021) is empirically superior to the more recent work BLT (Kong et al., 2022), the same observation as in (Jiang et al., 2022a) Table 2 Row 1 v.s. Row 8. We therefore did not experiment with BLT. Neither did we experiment with CGL-GAN (Zhou et al., 2022) or ICVT (Cao et al., 2022) due to their lack of bounding box category or text conditioning as input.

Evaluation metrics. (1) For the **realism** of generated layouts, we calculate the Fréchet distances (Heusel et al., 2017) between fake and real feature distributions. We consider two third-party feature spaces. One is the layout feature space pretrained by (Kikuchi et al., 2021). The other is the image feature space pretrained with the VGG network on ImageNet (Heusel et al., 2017). To obtain images according to generated layouts, we overlay foreground image patches and render foreground texts on top of background images. The rendering process is described under Figure 4. (2) For the **accuracy** of generated layouts w.r.t. their ground truth, we calculate the layout-to-layout IoU (Kikuchi et al., 2021) and DocSim (Patil et al., 2020). We skip their box-level matching process because the correspondences between generated and ground truth boxes are known through input conditions. (3) For the **regularity** of generated layouts, we reuse the overlap loss (Li et al., 2020) and misalignment loss (Li et al., 2020) in Section 3.3 as the metrics.

5.2. Ablation Study

Loss configurations. We establish from our multimodal conditioned version of LayoutGAN++ where we enable the original LayoutGAN++ (Kikuchi et al., 2021) to take background and foreground as inputs. We then progressively add on extra loss terms and report the quantitative measurements in Table 1 top session. We observe:

- (1) Comparing Row 1 and 2, all the metrics are improved, thanks to the enhanced controllability through the reconstruction of conditional inputs.
- (2) Comparing Row 2 and 3, unconditional discriminator benefits the layout regularity due to its approximation power between generated layout parameters and real regular ones.
- (3) Comparing Row 3 and 4, the supervised gIoU loss boosts the realism and accuracy by a significant margin, yet seemingly contradicts the regularity.
- (4) Fortunately, in Row 5, adding overlap loss and misalignment loss harmonizes all the metrics and achieves the optimum for each one. We name this "LayoutDETR-GAN (ours)" and stick to it for the following experiments.

Conditional embedding configurations. For foreground images, we do not consider this ablation study since the

Method	Realism		Accuracy		Regularity	
	Layout FID ↓	Image FID ↓	IoU ↑	DocSim ↑	Overlap ↓	Misalign (×10 ⁻²) ↓
Conditional LayoutGAN++	4.25	28.40	0.163	0.130	0.104	0.759
+ Gen. rec. (Eq. 9)	3.27	29.56	0.186	<u>0.148</u>	0.125	0.853
+ Uncond. dis. D^u	3.70	29.21	0.177	0.140	<u>0.103</u>	<u>0.681</u>
+ gIoU loss (Eq. 8)	<u>3.23</u>	<u>28.20</u>	0.182	0.138	0.106	0.721
+ Overlap & Misalign loss = LayoutDETR-GAN (ours)	3.19	27.35	0.208	0.151	0.101	0.646
- Text length embeddings	3.24	28.65	<u>0.191</u>	0.144	0.117	0.807
- Text class embeddings	25.17	29.25	0.166	0.132	0.110	0.000

Table 1. Ablation study w.r.t. loss config (top) or conditional embedding config (bottom) on **ads banner dataset**. Each row is progressively ablated from its row above. ↑/↓ indicates a higher/lower value is better. **Bold/underline** font indicates the top/second best value in the column.

embeddings are simply the image features. Whereas for foreground texts, we examine the importance of text length embeddings and text class embeddings by progressively removing them from the training. From Table 1 bottom session we observe:

- (1) Comparing Row 5 and 6, text length embeddings are beneficial all around. We reason that text length is a strong indicator of a proper text box size. This validates the strong positive correlation between text lengths and box sizes.
- (2) Comparing Row 6 and 7, text label embeddings serve as an essential role in the generation. LayoutFID deteriorates significantly without text label embeddings (Row 7) due to the phenomenon that boxes of similar texts tend to collapse to the same regions (referring to the 0.0 misalignment). This implies that text contents themselves are not as discriminative as text labels to differentiate box parameters. This also explains why a variety of layout datasets and models have to involve box labels.

5.3. Comparisons to baselines

Quantitative comparisons are reported in Table 2. We involve three of our alternative model variants: GAN-, VAE-, and VAE-GAN-based. For more intuitive understanding of the tables, we visualize the numbers per row into a radar plot in Figure 3. Each corner of the radar plot corresponds to a metric. We observe:

- (1) On our ads banner dataset, at least one of our variants outperforms all the baselines in terms of realism and accuracy. Our LayoutDETR-GAN achieves the second best in terms of regularity. The margin to the best baseline is minor. This evidences the efficacy of our understanding of multi-modality and sophisticated loss configurations.
- (2) On CLAY dataset, at least one of our variants outperforms all the baselines for all the metrics. Our efficacy generalizes in at least these two multimodal domains.
- (3) According to the radar plots on both datasets, our LayoutDETR-GAN variant (the third to the right) achieves near-top overall measures with the most balanced perfor-

LayoutDETR: Detection Transformer Is a Good Multimodal Layout Designer

Method	Ads banner dataset						CLAY mobile application UI dataset					
	Realism		Accuracy		Regularity		Realism		Accuracy		Regularity	
	Layout FID ↓	Image FID ↓	IoU ↑	DocSim ↑	Overlap ↓	Misalign ($\times 10^{-2}$) ↓	Layout FID ↓	Image FID ↓	IoU ↑	DocSim ↑	Overlap ↓	Misalign ($\times 10^{-2}$) ↓
LayoutGAN++ (Kikuchi et al., 2021)	4.25	28.40	0.163	0.130	0.104	0.759	14.12	7.49	0.049	0.078	0.817	1.057
READ (Patil et al., 2020)	4.45	32.10	0.177	0.141	0.093	2.867	3.68	5.38	<u>0.312</u>	<u>0.121</u>	<u>0.099</u>	2.045
Vinci (Guo et al., 2021)	38.97	58.12	0.104	0.143	0.243	0.271	22.98	13.04	0.178	0.104	0.253	2.526
LayoutTransformer (Gupta et al., 2021)	5.47	39.70	0.080	0.115	0.127	3.632	<u>2.64</u>	<u>5.27</u>	0.216	0.106	0.357	0.833
LayoutDETR-GAN (ours)	3.19	27.35	0.208	<u>0.151</u>	<u>0.101</u>	<u>0.646</u>	1.84	5.22	0.261	0.113	0.083	<u>0.773</u>
LayoutDETR-VAE (ours)	3.25	<u>27.47</u>	0.216	0.152	0.119	1.737	4.99	5.49	0.327	0.123	0.205	5.119
LayoutDETR-VAE-GAN	<u>3.23</u>	27.88	<u>0.210</u>	<u>0.151</u>	0.117	1.439	3.98	5.87	0.158	0.108	0.148	0.691

Table 2. Quantitative comparisons to baselines. \uparrow/\downarrow indicates a higher/lower value is better. **Bold/underline** font indicates the top/second best value in the column.

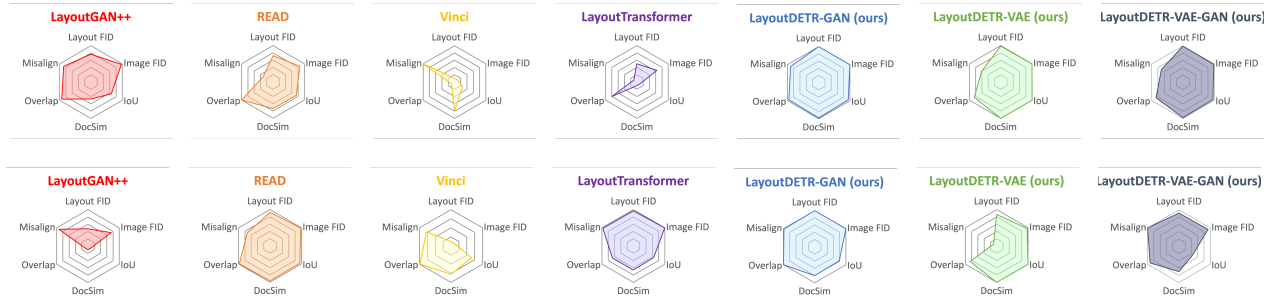


Figure 3. Radar plots for Table 2 on our ads banner dataset (top) and CLAY mobile application UI dataset (bottom). Each plot corresponds to a row (method) in the table. Each corner in a plot corresponds to a column (metric) in the table. Values are normalized to the unit range, the higher the better.

mance. We therefore apply this variant for the following system design and user study. READ achieves similarly balanced performance on the CLAY dataset, while the other baselines always miss at least one measurement by a significant margin. This is due to their generators by nature not being designed for multimodal conditions.

Qualitative comparisons are in Figure 4. We observe:

- (1) For the ads banner dataset, our designs understand the background the most effectively. For example, they never overlay foreground elements on top of clutter background subregions. If the backgrounds look symmetric, our layouts are also replaced in the middle of the banners.
- (2) For the ads banner dataset, our designs also approximate the real layout distribution the most closely. For example, the relative font sizes (box sizes) and distances (box distances) in our layouts look the most reasonable.
- (3) CLAY dataset is more challenging in terms of multimodal conditioning, as it has more tiny foreground elements. Still, our layouts appear the best aligned and least overlapping, with reasonable designs to harmonize with backgrounds, although different from the ground truth.

See more visual results in the supplementary video.

5.4. Graphical System Design and User Study

We further build our generator into a graphical system for user-friendly service in practice. See Section D and Fig-

ure 7 in the supplementary material for the step-by-step UI designs. More live demonstrations are nested in our supplementary video.

With the graphical system, we can test a massive number of cases and collect generation results in the wild. This facilitates us to conduct user study about users' subjective preferences for our designs. In specific, we collected 811 testing samples and our rendered results via the graphical system. Then we tested the four aforementioned baseline generators with the same testing inputs. We configured a binary comparison task between our result and each of the baseline results for each sample. We intentionally avoided comparisons among more than two methods. This is because (1) we are not interested in the comparisons among baselines and (2) extra unnecessary complexity would distract users' attention. In total, we launched $811 \times 4 = 3,244$ jobs on AMT, and assigned three random workers for each job. We simply asked each worker which of the two designs they prefer. We intentionally did not pre-define any criterion for the preference so as to fully respect their subjective judgments. There were 143 workers involved in our study. On average each worker completed 149 jobs, each in 47 seconds. All of the workers have an approval rate history above 90% on AMT. We did not set any restrictions for workers' gender, race, sexuality, demographics, locations, remuneration rates, etc. Our user study has been reviewed and approved by our ethical board.

Table 3 lists the ratio of users' preferences to our designs

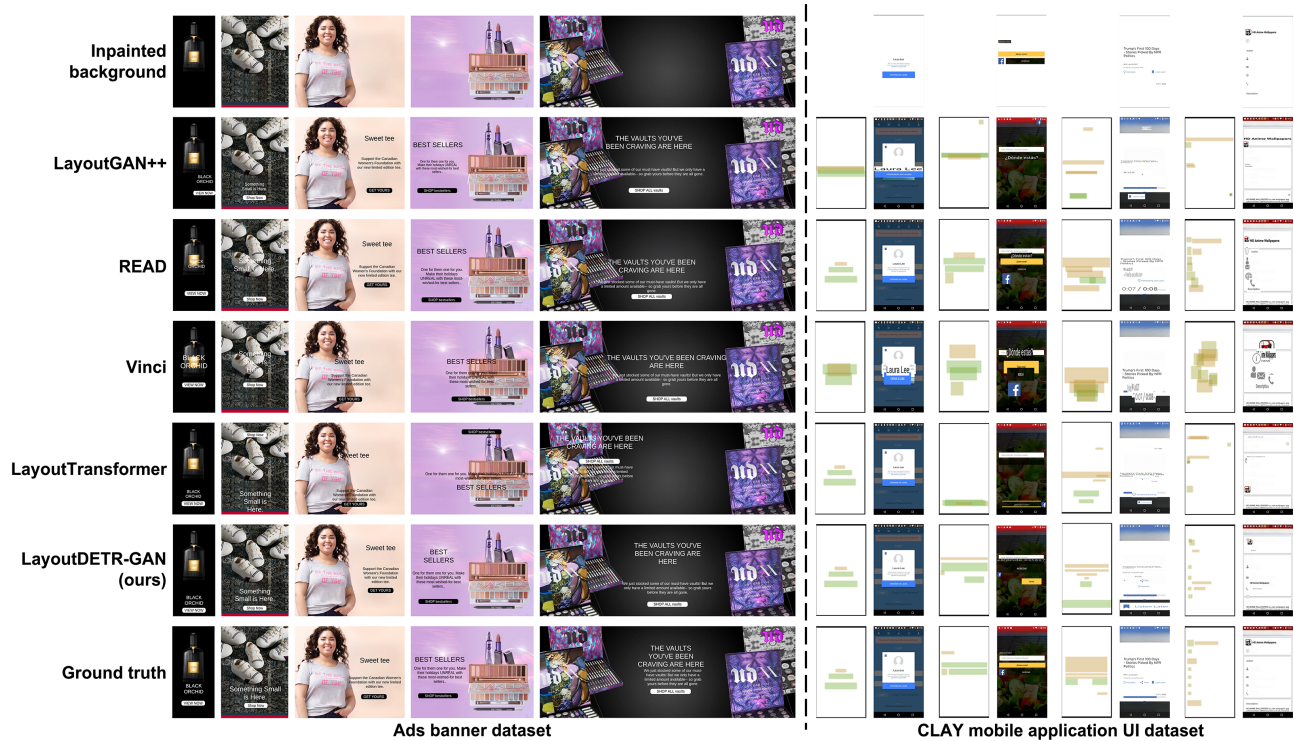


Figure 4. **Left:** visual comparisons on our **ads banner dataset**. Samples are from the testing set and not cherry-picked. The same rendering process applies to all the methods: (1) Text font sizes are adaptively determined so as to tightly fit into their inferred boxes. (2) Text font colors and button pad colors are adaptively determined to be either black or white whichever contrasts more with the background. (3) Button text colors are then determined to contrast with the button pads. (4) Text font styles are constantly set as *Arial*. (5) Boxes are enforced to horizontally center-align with each other. **Right:** visual comparisons on **CLAY mobile application UI dataset**. Each odd column stands for the generated graphic layouts. Each even column stands for the rendered images with foreground elements resized and overlaid following the layouts.

Method	Ratio of preferences to LayoutDETR-GAN (ours) [p-value]
LayoutGAN++ (Kikuchi et al., 2021)	54.2% [2e-5]
READ (Patil et al., 2020)	54.2% [2e-5]
Vinci (Guo et al., 2021)	61.8% [1e-31]
LayoutTransformer (Gupta et al., 2021)	65.5% [1e-53]

Table 3. User preferences on our **ads banner dataset** between samples generated by two methods, and their statistical significance measured by p-values.

against each baseline. To quantize the statistical significance of our user study, we also calculate the p-value of a null hypothesis that the results of binary comparisons are equivalent to tossing a fair coin. It is calculated via the cumulative distribution function of the binomial distribution, the smaller the more statistically significant.

According to Table 3, all the ratios are above 50%, meaning a majority of users prefer our designs over any baseline. These preferences are statistically significant, as all the p-values are far below 0.05. This means users’ preferences are contrary to random tosses of a fair coin. As a result,

our layout designs are validated more appealing to human judgments. This benefits from our effective approximation of real layout distributions and understanding of multimodal conditions.

6. Conclusion

We present LayoutDETR for customizable layout design. It inherits the high quality and realism of generative models, and benefits from object detectors to understand multimodal conditions. Experiments validate that our solution yields new state-of-the-art performance for layout generation on a new ads banner dataset and beyond. For practical usage, we implement our solution as a graphical system that facilitates user study. We witness a majority of users’ subjective preferences for our designs against several recent works.

Future work includes: (1) exploring diffusion denoising probability models (DDPM) (Ho et al., 2020; Song et al., 2021; Nichol et al., 2022; Rombach et al., 2022) for layout generation; (2) establishing datasets that benchmark multimodal layout generation for 2D/3D natural scenes.

Acknowledgement

We thank Abigail Kuttruff, Brian Brechbuhl, Bram Wallace, Mingfei Gao, and De Wang for constructive advice.

References

- Arroyo, D. M., Postels, J., and Tombari, F. Variational transformer networks for layout generation. *CVPR*, 2021.
- Bello, I., Zoph, B., Vaswani, A., Shlens, J., and Le, Q. V. Attention augmented convolutional networks. *ICCV*, 2019.
- Brock, A., Donahue, J., and Simonyan, K. Large scale gan training for high fidelity natural image synthesis. *ICLR*, 2019.
- Cao, Y., Ma, Y., Zhou, M., Liu, C., Xie, H., Ge, T., and Jiang, Y. Geometry aligned variational transformer for image-conditioned layout generation. *Multimedia*, 2022.
- Carion, N., Massa, F., Synnaeve, G., Usunier, N., Kirillov, A., and Zagoruyko, S. End-to-end object detection with transformers. *ECCV*, 2020.
- Caron, M., Misra, I., Mairal, J., Goyal, P., Bojanowski, P., and Joulin, A. Unsupervised learning of visual features by contrasting cluster assignments. 2020.
- Chen, G., Xie, P., Dong, J., and Wang, T. Understanding programmatic creative: The role of ai. *Journal of Advertising*, 2019.
- Chen, X., Mishra, N., Rohaninejad, M., and Abbeel, P. Pixelsnail: An improved autoregressive generative model. *ICML*, 2018.
- Dai, Z., Cai, B., Lin, Y., and Chen, J. Up-detr: Unsupervised pre-training for object detection with transformers. *CVPR*, 2021.
- Deka, B., Huang, Z., Franzen, C., Hibsichman, J., Afergan, D., Li, Y., Nichols, J., and Kumar, R. Rico: A mobile app dataset for building data-driven design applications. *UIST*, 2017.
- Devlin, J., Chang, M.-W., Lee, K., and Toutanova, K. Bert: Pre-training of deep bidirectional transformers for language understanding. *NAACL*, 2019.
- Girshick, R. Fast r-cnn. *ICCV*, 2015.
- Goodfellow, I., Pouget-Abadie, J., Mirza, M., Xu, B., Warde-Farley, D., Ozair, S., Courville, A., and Bengio, Y. Generative adversarial networks. *NeurIPS*, 2014.
- Guo, S., Jin, Z., Sun, F., Li, J., Li, Z., Shi, Y., and Cao, N. Vinci: an intelligent graphic design system for generating advertising posters. *CHI*, 2021.
- Gupta, K., Lazarow, J., Achille, A., Davis, L. S., Mahadevan, V., and Shrivastava, A. Layouttransformer: Layout generation and completion with self-attention. *ICCV*, 2021.
- Haykin, S. and Network, N. A comprehensive foundation. *Neural networks*, 2004.
- He, K., Gkioxari, G., Dollár, P., and Girshick, R. Mask r-cnn. *ICCV*, 2017.
- He, K., Chen, X., Xie, S., Li, Y., Dollár, P., and Girshick, R. Masked autoencoders are scalable vision learners. *CVPR*, 2022.
- Heusel, M., Ramsauer, H., Unterthiner, T., Nessler, B., and Hochreiter, S. Gans trained by a two time-scale update rule converge to a local nash equilibrium. *NeurIPS*, 2017.
- Ho, J., Jain, A., and Abbeel, P. Denoising diffusion probabilistic models. *NeurIPS*, 2020.
- Hochreiter, S. and Schmidhuber, J. Long short-term memory. *Neural computation*, 1997.
- Hussain, Z., Zhang, M., Zhang, X., Ye, K., Thomas, C., Agha, Z., Ong, N., and Kovashka, A. Automatic understanding of image and video advertisements. *CVPR*, 2017.
- Jiang, Z., Deng, H., Wu, Z., Guo, J., Sun, S., Mijovic, V., Yang, Z., Lou, J.-G., and Zhang, D. Unilayout: Taming unified sequence-to-sequence transformers for graphic layout generation. *arXiv*, 2022a.
- Jiang, Z., Sun, S., Zhu, J., Lou, J.-G., and Zhang, D. Coarse-to-fine generative modeling for graphic layouts. *AAAI*, 2022b.
- Jyothi, A. A., Durand, T., He, J., Sigal, L., and Mori, G. Layoutvae: Stochastic scene layout generation from a label set. *ICCV*, 2019.
- Karras, T., Aila, T., Laine, S., and Lehtinen, J. Progressive growing of gans for improved quality, stability, and variation. *ICLR*, 2018.
- Karras, T., Laine, S., and Aila, T. A style-based generator architecture for generative adversarial networks. *CVPR*, 2019.
- Karras, T., Laine, S., Aittala, M., Hellsten, J., Lehtinen, J., and Aila, T. Analyzing and improving the image quality of stylegan. *CVPR*, 2020.
- Kikuchi, K., Simo-Serra, E., Otani, M., and Yamaguchi, K. Constrained graphic layout generation via latent optimization. *ACM MM*, 2021.

- Kingma, D. P. and Ba, J. Adam: A method for stochastic optimization. *ICLR*, 2015.
- Kingma, D. P. and Welling, M. Auto-encoding variational bayes. *ICLR*, 2013.
- Kipf, T. N. and Welling, M. Semi-supervised classification with graph convolutional networks. *ICLR*, 2017.
- Kong, X., Jiang, L., Chang, H., Zhang, H., Hao, Y., Gong, H., and Essa, I. Blt: Bidirectional layout transformer for controllable layout generation. *ECCV*, 2022.
- Krizhevsky, A., Sutskever, I., and Hinton, G. E. Imagenet classification with deep convolutional neural networks. *NeurIPS*, 2012.
- Landa, R. Graphic design solutions/robin landa. *Wadsworth, Boston*, 2010.
- Larsen, A. B. L., Sønderby, S. K., Larochelle, H., and Winther, O. Autoencoding beyond pixels using a learned similarity metric. *ICML*, 2016.
- Lee, D., Liu, S., Gu, J., Liu, M.-Y., Yang, M.-H., and Kautz, J. Context-aware synthesis and placement of object instances. *NeurIPS*, 2018.
- Lee, H.-Y., Jiang, L., Essa, I., Le, P. B., Gong, H., Yang, M.-H., and Yang, W. Neural design network: Graphic layout generation with constraints. *ECCV*, 2020.
- Lee, K., Chang, H., Jiang, L., Zhang, H., Tu, Z., and Liu, C. Vitgan: Training gans with vision transformers. *ICLR*, 2022.
- Li, G., Baechler, G., Tragut, M., and Li, Y. Learning to denoise raw mobile ui layouts for improving datasets at scale. *CHI*, 2022a.
- Li, J., Yang, J., Hertzmann, A., Zhang, J., and Xu, T. Layoutgan: Generating graphic layouts with wireframe discriminators. *ICLR*, 2019.
- Li, J., Yang, J., Zhang, J., Liu, C., Wang, C., and Xu, T. Attribute-conditioned layout gan for automatic graphic design. *TVCG*, 2020.
- Li, J., Li, D., Xiong, C., and Hoi, S. Blip: Bootstrapping language-image pre-training for unified vision-language understanding and generation. *ICML*, 2022b.
- Lin, T.-Y., Goyal, P., Girshick, R., He, K., and Dollár, P. Focal loss for dense object detection. *ICCV*, 2017.
- Liu, B., Zhu, Y., Song, K., and Elgammal, A. Towards faster and stabilized gan training for high-fidelity few-shot image synthesis. *ICLR*, 2020.
- Liu, S., Li, F., Zhang, H., Yang, X., Qi, X., Su, H., Zhu, J., and Zhang, L. Dab-detr: Dynamic anchor boxes are better queries for detr. *ICLR*, 2022.
- Lok, S. and Feiner, S. A survey of automated layout techniques for information presentations. *Proceedings of SmartGraphics*, 2001.
- Meng, D., Chen, X., Fan, Z., Zeng, G., Li, H., Yuan, Y., Sun, L., and Wang, J. Conditional detr for fast training convergence. *ICCV*, 2021.
- Nguyen, D. D., Nepal, S., and Kanhere, S. S. Diverse multimedia layout generation with multi choice learning. *Multimedia*, 2021.
- Nichol, A., Dhariwal, P., Ramesh, A., Shyam, P., Mishkin, P., McGrew, B., Sutskever, I., and Chen, M. Glide: Towards photorealistic image generation and editing with text-guided diffusion models. *ICML*, 2022.
- Parmar, N., Vaswani, A., Uszkoreit, J., Kaiser, L., Shazeer, N., Ku, A., and Tran, D. Image transformer. *ICML*, 2018.
- Patil, A. G., Ben-Eliezer, O., Perel, O., and Averbuch-Elor, H. Read: Recursive autoencoders for document layout generation. *CVPR Workshops*, 2020.
- Redmon, J. and Farhadi, A. Yolo9000: better, faster, stronger. *CVPR*, 2017.
- Redmon, J., Divvala, S., Girshick, R., and Farhadi, A. You only look once: Unified, real-time object detection. *CVPR*, 2016.
- Ren, S., He, K., Girshick, R., and Sun, J. Faster r-cnn: Towards real-time object detection with region proposal networks. *NeurIPS*, 2015.
- Rezatofighi, H., Tsoi, N., Gwak, J., Sadeghian, A., Reid, I., and Savarese, S. Generalized intersection over union: A metric and a loss for bounding box regression. *CVPR*, 2019.
- Rezende, D. J., Mohamed, S., and Wierstra, D. Stochastic backpropagation and approximate inference in deep generative models. *ICML*, 2014.
- Rombach, R., Blattmann, A., Lorenz, D., Esser, P., and Ommer, B. High-resolution image synthesis with latent diffusion models. *CVPR*, 2022.
- Salimans, T., Karpathy, A., Chen, X., and Kingma, D. P. Pixelcnn++: Improving the pixelcnn with discretized logistic mixture likelihood and other modifications. *ICLR*, 2017.
- Sauer, A., Schwarz, K., and Geiger, A. Stylegan-xl: Scaling stylegan to large diverse datasets. *SIGGRAPH*, 2022.

- Simonyan, K. and Zisserman, A. Very deep convolutional networks for large-scale image recognition. *ICLR*, 2015.
- Socher, R., Lin, C. C., Manning, C., and Ng, A. Y. Parsing natural scenes and natural language with recursive neural networks. *ICML*, 2011.
- Socher, R., Perelygin, A., Wu, J., Chuang, J., Manning, C. D., Ng, A. Y., and Potts, C. Recursive deep models for semantic compositionality over a sentiment treebank. *EMNLP*, 2013.
- Song, J., Meng, C., and Ermon, S. Denoising diffusion implicit models. *ICLR*, 2021.
- Stribley, M. Rules of composition all designers live by. Retrieved May, 2016.
- Suvorov, R., Logacheva, E., Mashikhin, A., Remizova, A., Ashukha, A., Silvestrov, A., Kong, N., Goka, H., Park, K., and Lempitsky, V. Resolution-robust large mask inpainting with fourier convolutions. *WACV*, 2022.
- Tan, F., Bernier, C., Cohen, B., Ordonez, V., and Barnes, C. Where and who? automatic semantic-aware person composition. *WACV*, 2018.
- Van den Oord, A., Kalchbrenner, N., Espeholt, L., Vinyals, O., Graves, A., et al. Conditional image generation with pixelcnn decoders. *NeurIPS*, 2016.
- Vaswani, A., Shazeer, N., Parmar, N., Uszkoreit, J., Jones, L., Gomez, A. N., Kaiser, Ł., and Polosukhin, I. Attention is all you need. *NeurIPS*, 2017.
- Wang, X., Girshick, R., Gupta, A., and He, K. Non-local neural networks. *CVPR*, 2018.
- Wang, Y., Pu, G., Luo, W., Wang, Y., Xiong, P., Kang, H., and Lian, Z. Aesthetic text logo synthesis via content-aware layout inferring. *CVPR*, 2022.
- Xie, Y., Huang, D., Wang, J., and Lin, C.-Y. Canvasemb: learning layout representation with large-scale pre-training for graphic design. *Multimedia*, 2021.
- Yamaguchi, K. Canvasvae: learning to generate vector graphic documents. *ICCV*, 2021.
- Yu, F., Liu, K., Zhang, Y., Zhu, C., and Xu, K. Partnet: A recursive part decomposition network for fine-grained and hierarchical shape segmentation. *CVPR*, 2019.
- Yu, J., Li, X., Koh, J. Y., Zhang, H., Pang, R., Qin, J., Ku, A., Xu, Y., Baldrige, J., and Wu, Y. Vector-quantized image modeling with improved vqgan. *ICLR*, 2022.
- Yu, N., Li, K., Zhou, P., Malik, J., Davis, L., and Fritz, M. Inclusive gan: Improving data and minority coverage in generative models. *ECCV*, 2020.
- Yu, N., Liu, G., Dundar, A., Tao, A., Catanzaro, B., Davis, L. S., and Fritz, M. Dual contrastive loss and attention for gans. *ICCV*, 2021.
- Zhao, H., Shen, X., Lin, Z., Sunkavalli, K., Price, B., and Jia, J. Compositing-aware image search. *ECCV*, 2018.
- Zheng, X., Qiao, X., Cao, Y., and Lau, R. W. Content-aware generative modeling of graphic design layouts. *TOG*, 2019.
- Zhong, X., Tang, J., and Yepes, A. J. Publaynet: largest dataset ever for document layout analysis. *ICDAR*, 2019.
- Zhou, M., Xu, C., Ma, Y., Ge, T., Jiang, Y., and Xu, W. Composition-aware graphic layout gan for visual-textual presentation designs. *IJCAI*, 2022.

LayoutDETR: Detection Transformer Is a Good Multimodal Layout Designer

Method	Domain(s)	Conditioning modality(ies)	Generative model(s)	Architecture(s)
LayoutGAN (Li et al., 2019)	Graphics	Bbox category	GAN	MLP, CNN
LayoutGAN+ (Li et al., 2020)	Graphics	Bbox category, attribute vector	GAN	MLP, CNN
LayoutGAN++ (Kikuchi et al., 2021)	Graphics	Bbox category	GAN	Transformer
LayoutVAE (Jyothi et al., 2019)	Natural scenes	Bbox category	VAE	MLP
READ (Patil et al., 2020)	Graphics	Bbox category	VAE	RvNN
Vinci (Guo et al., 2021)	Graphics	Bbox category, bg/fg images, texts	VAE	LSTM
NDN (Lee et al., 2020)	Graphics	Bbox category, spatial relation	VAE	GCN
VTN (Arroyo et al., 2021)	Graphics, natural scenes	Bbox category	VAE	Transformer
CanvasVAE (Yamaguchi, 2021)	Graphics	Bbox category, attribute vector	VAE	Transformer
C2F-VAE (Jiang et al., 2022b)	Graphics	Bbox category	VAE	Transformer
ContentGAN (Zheng et al., 2019)	Graphics	Bbox category, fg images, texts	VAE + GAN	Transformer
TextLogoLayout (Wang et al., 2022)	Graphics	Glyph	VAE + GAN	RNN, CNN
LayoutMCL (Nguyen et al., 2021)	Graphics	Bbox category	ARM	RNN, CNN
CanvasEmb (Xie et al., 2021)	Graphics	Bbox category, attribute vector	ARM	Transformer
LayoutTransformer (Gupta et al., 2021)	Graphics, natural scenes, 3D	Bbox category	ARM	Transformer
BLT (Kong et al., 2022)	Graphics, natural scenes, 3D	Bbox category	ARM	Transformer
UniLayout (Jiang et al., 2022a)	Graphics	Bbox category	ARM	Transformer
CGL-GAN (Zhou et al., 2022)	Graphics	Bg image	GAN + DETR	Transformer
ICVT (Cao et al., 2022)	Graphics	Bg image	VAE + DETR	Transformer
LayoutDETR-GAN (ours)	Graphics	Bbox category, bg/fg images, texts	GAN + DETR	Transformer
LayoutDETR-VAE (ours)	Graphics	Bbox category, bg/fg images, texts	VAE + DETR	Transformer
LayoutDETR-VAE-GAN (ours)	Graphics	Bbox category, bg/fg images, texts	VAE + GAN + DETR	Transformer

Table 4. A taxonomy of existing and our layout generation methods. We tag for each method its working data domain(s), data modality(ies) of input condition(s), backend generative model type(s), as well as implementation architecture(s).

A. Taxonomy of Layout Generation Methods

Table 4 summarizes the key features of existing layout generation methods and ours. Our method and its variants are the only ones that enable full control of varying multimodal conditions, and only a few that integrate object detection techniques into layout generation.

B. Implementation Details

Architecture design is where we integrate object detection with layout generation. Detection transformer (DETR) architecture (Carion et al., 2020) is employed and modified for LayoutDETR generator G and conditional discriminator D^c . It targets to boost the understanding of background from the perspective of visual detection, and enhance the controllability of background on the layout.

As depicted in Figure 2 bottom left in the main paper, G and D^c contain a visual transformer encoder for background understanding and a transformer decoder for layout generation. The encoder part is the same as in DETR (Carion et al., 2020), and is identical in G and D^c . It consists of a CNN backbone that extracts a compact feature representation from a background image, as well as a multi-head visual transformer (ViT) encoder (Wang et al., 2018; He et al., 2022) that incorporates positional encoding inputs (Parmar et al., 2018; Bello et al., 2019). It outputs tokenized visual features for cross-attention in the following layout transformer decoder.

The layout decoder is also inherited from the DETR transformer decoder with self-attention and encoder-decoder-cross-attention mechanisms (Vaswani et al., 2017). It transforms each of the N input embeddings (corresponding to N foreground elements) into layout bounding box parameters. Our architecture differs from DETR where we have users’ foreground elements as inputs to drive the transformation, while DETR does not. Therefore, we replace their freely-learnable object queries with our foreground embeddings as the input tokens to the decoder, which are detailed below.

Foreground elements are composed of texts $\mathcal{T} = \{\mathbf{t}^i\}_{i=1}^M = \{(\mathbf{s}^i, c^i, l^i)\}_{i=1}^M$ and image patches $\mathcal{P} = \{\mathbf{p}^i\}_{i=1}^K$. Thence, each foreground embedding is a concatenation of noise embedding and either text embedding or image embedding. To calculate the text embedding, we separately encode text string, text class, and text length, and concatenate the features together. The text string is encoded by the pretrained and fixed BERT text encoder (Devlin et al., 2019). The text class and quantized text length are encoded by learning a dictionary. To calculate the image embedding, we use the same ViT as used for background encoding. The weights are shared and initialized by the Up-DETR-pretrained model (Dai et al., 2021).

For the other networks F^c , D^u , F^u , E , and R that do not take background images as an input condition, we simply use the

above transformer decoder architecture as their implementations. For foreground image reconstruction layers in F^c and R , we employ the StyleGAN2 image generator architecture (Karras et al., 2020). For text string reconstruction layers, we employ the pretrained BERT language model decoder (Devlin et al., 2019; Li et al., 2022b). For text class and text length decoding layers, we use 3-layer MLPs.

We implement LayoutDETR in PyTorch and use Adam optimizer (Kingma & Ba, 2015) to train the models on 8 NVIDIA A100 GPUs. Without losing generality, background images are downsized to 256×256 for our ads banner dataset and 960×540 for CLAY dataset. We set batch size as 16, constant learning rate as 10^{-5} , and keep training for 500k iterations.

C. Details of Ads Banner Dataset Collection

The sources of raw ads banner images consist of two parts. First, we manually went through all the images in Pitt Image Ads Dataset (Hussain et al., 2017). We filtered out those with single modality, low quality, or old-fashioned designs. We then selected 3,536 valid ads banner images. Second, we searched on Google Image Search Engine with the keywords "XXX ads banner" where "XXX" goes through a list of 2,765 retailer brand names including the Fortune 500 brands. For each keyword search, we crawled the top 20 results and manually filtered out non-ads, single-modality, low-quality, or offensive-content images. We then selected 4,321 valid ads banner images. Combining the two sources, we in total obtained 7,857 valid ads banner images with arbitrary sizes.

Next, we crowdsourced on Amazon Mechanical Turk (AMT)² to obtain human annotations for the bounding box and class of each text phrase in each image. The class space spans over 11 categories as shown in the AMT interface in Figure 5 top. Without losing representativeness, we focus on the top-4 most common categories in this work: $\{header, body\ text, disclaimer / footnote, button\}$. We also linked a detailed instructional document with examples for workers to fully understand the annotation task. See the instruction in Figure 5 bottom. We assigned each annotation job to three workers. For the final annotation results, we averaged over three workers' submissions and incorporated our judgments for the tie cases. In total there were 67 workers involved in the task. On average each worker submitted 314 jobs in around 3 minutes per job. All of the workers have an approval rate history above 90% on AMT. We did not set any restrictions for workers' gender, race, sexuality, demographics, locations, remuneration rates, etc. Our annotation process has been reviewed and approved by our ethical board.

After annotation, it is necessary to reverse the design by separating foreground elements from background images to configure the training/testing data. We apply a modern optical character recognition (OCR) technique³ to extract the text inside each bounding box, and adopt a modern image inpainting technique (Suvorov et al., 2022) to erase the texts. The separation of texts from background images is exemplified in Figure 6. After filtering out a few samples with undesirable OCR or inpainting results, we finally obtain 7,196 valid samples for the following experiments.

It is worth noting that inpainting clues may leak the layout bounding box ground truth information and shortcut training. Therefore, during training, we intentionally inpaint background images at additional random subregions that are irrelevant to their layouts.

D. Graphical System Step-by-Step Designs

Since we validate that our solution sets up a new state of the art for multimodal layout design, it is worth encapsulating it into a graphical system for user-friendly service in practice. Figure 7 demonstrates our step-by-step UI designs. In specific:

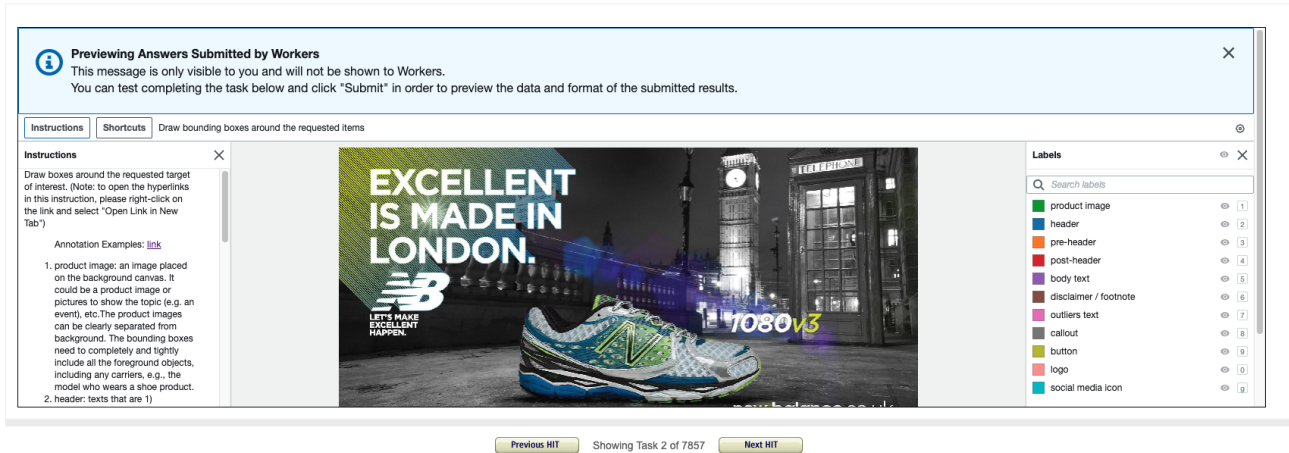
(1) Figure 7(a) shows the initial page that allows users to customize their background images and optionally foreground elements: *header text*, *body text*, *footnote/disclaimer text*, *button text*, as well as *button border radius* (zero radius means a rectangular button). Text colors, button pad color, and text fonts can be customized.

(2) Once users update their background and foreground elements, they are previewed on the right part of the same page, as shown in Figure 7(b). The locations and sizes of foreground elements in the preview are meaningless, yet they just conceptually show what contents are going to be rendered on top of the background.

(3) Once users click "Next", it moves on to the next page with our design results, as shown in Figure 7(c). Given one layout designed in the backend, we post-process it by randomly jittering the generated box parameters by 20% while keeping the original non-overlapping and alignment regularity.

²<https://www.mturk.com/>

³<https://github.com/PaddlePaddle/PaddleOCR>



(a) AMT interface



Product image: need to completely and tightly include all the foreground objects, cannot go outside the banner canvas

(b) Instructional example

Figure 5. **Top:** AMT interface with instructions on the left for users to annotate the bounding box and class of each existing copywriting text on each image. **Bottom:** one instructional example of the definitions of text bounding boxes and text classes.

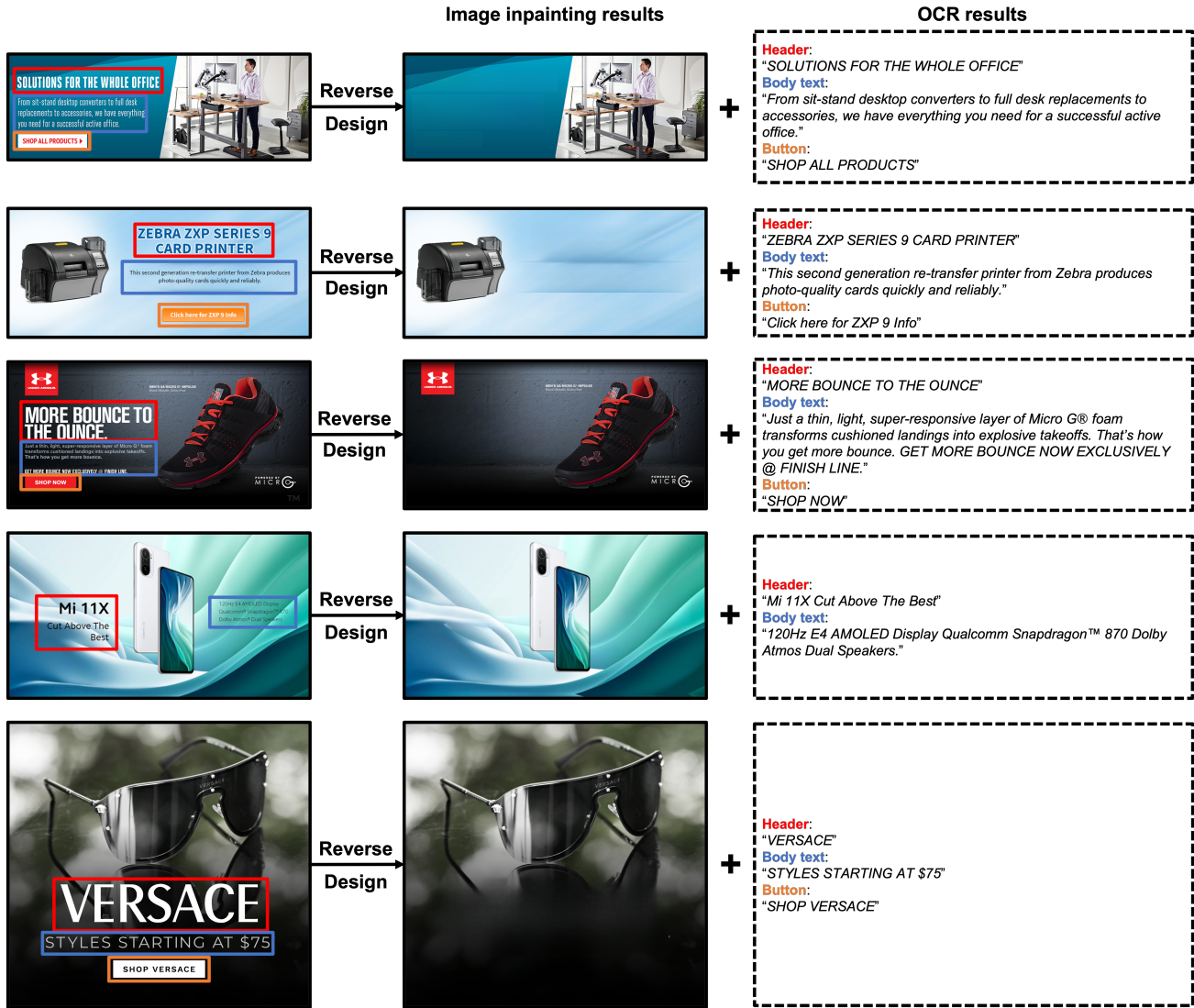


Figure 6. Reverse engineering examples of separating foreground elements from background images using OCR and image inpainting techniques.

LayoutDETR: Detection Transformer Is a Good Multimodal Layout Designer

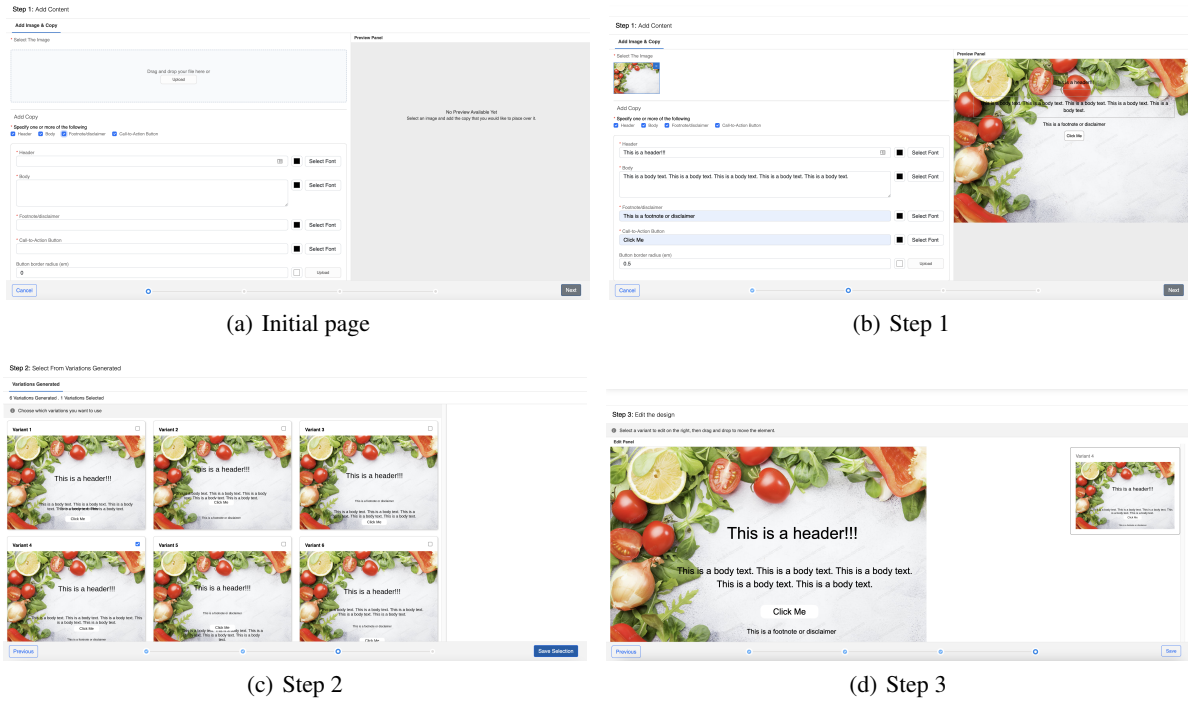


Figure 7. Step-by-step usage of our graphical system for customizable multimodal graphic layout design.

(4) Afterwards, the system renders foreground elements given the layout bounding boxes. The text font sizes and line breakers are adaptively determined so as to tightly squeeze into the boxes. Considering *header texts* usually have short strings yet are assigned with large boxes, their font sizes are naturally large enough. We showcase six of our rendered results on this page, and allow users to select one or more satisfactory designs.

(5) Once users make their selection(s) and click "Save Selection", it moves onto the last page as shown in Figure 7(d). On this page, users are allowed to manually customize the size and location of each rendered foreground element. Once they finish, they click "Save" to exit our system.

More live demonstrations are nested in our supplementary video.